Design of a Magnetic Field Modulated Screw Containing Composite Rotors for Wave Energy Conversion

Tao Xia, Zihao Li, Haitao Liu, Yangfei Zhang, and Haitao Yu

***Abstract*—A segmented modulated magnetic lead screw (SMMLS) is designed and analyzed in this article. SMMLS consists of three coaxial tubular components, including an internal stator composed of circular ring permanent magnets (PMs), an intermediate spiral modulation ring composed of ferromagnetic materials, and an external rotor composed of segmented spiral PMs embedded in a nonmagnetic frame. This device adopts magnetic transmission technology, which can convert low-speed linear motion into high-speed rotary motion. Compared with the existing magnetic lead screw (MLS) and magnetic field modulated screw (MFMS), the segmented helical PMs on the outer rotor of SMMLS can form a composite rotor nested with the motor. Furthermore, the inner stator PMs of SMMLS have a circular structure, which reduces the difficulty of manufacturing. The middle part of SMMLS can perform linear motion without PMs, which converts low-speed high-thrust linear motion into high-speed rotational motion, making it ideal for low-speed high-thrust long-stroke applications, such as wave power generation. Then, a prototype of the MLS was built to verify its magnetic transfer capability. Simulations and experiments verify the effectiveness of SMMLS for wave energy conversion.**

***Index Terms*—High gear ratio, magnetic field modulation, magnetic lead screw (MLS), wave energy conversion.**

I. Introduction

MAGNETIC actuators realize energy transmission through nonmechanical contact magnetic field coupling compared with mechanical coupling as they avoid problems such as mechanical abrasion, jamming, and insufficient overload capacity, reduce mechanical noise, and improve operational reliability [1], [2], [3]. As early as in the 1940s, the American scholar H. T. Faus [4] proposed the prototype of magnetic transmission, i.e., the use of permanent magnetic field coupling on the driving and driven wheels to realize energy transmission. However, due to the limitations of magnetic material performance and processing technology at that time, high-performance transmission could not be realized. In recent years, with the development of high-performance magnetic material processing technology, the transmission performance of magnetic transmission equipment has been significantly improved. In addition, the development of magnetic field modulation technology has further improved the torque or thrust density of magnetic transmission [5], [6], [7]. In 2001, Atallah et al. [8] proposed a concentric rotating magnetic gear (RMG) structure, which consists of an inner rotor, an outer rotor, and a magnetic adjusting ring. The magnetic adjustment ring is placed between the inner and outer rotors to change the air gap magnetic conductivity, thereby affecting the distribution of the air gap magnetic field, and achieving harmonic speed change and torque transmission in the magnetic field space. British scholars extended the magnetic transmission technology to the field of linear actuators and proposed a cylindrical linear magnetic gear (LMG) structure. The inner and outer magnetic poles and magnetic adjustment rings are distributed axially, and the magnetic adjustment ring is still placed between the inner and outer actuators to change the air gap magnetic conductivity. Through magnetic field modulation, variable speed and thrust transmission are achieved, and the thrust density of the LMG can reach 1.7 MN/m^3, However, due to the opposite direction of internal and external motion, the size and weight of LMG are relatively large [9], [10]. The above studies can only achieve a single degree of freedom magnetic transmission. Vitale et al. [11] proposed the prototype of a magnetic lead screw (MLS) in 1998, which can convert rotary motion into linear motion through magnetic transmission, and applied it to the field of heart pumps, achieving multidegree of freedom magnetic transmission and expanding the application range of magnetic transmission technology. In 2011, Wang et al. [12] first proposed a high-thrust density permanent magnet (PM) screw linear actuator. The electromagnetic force analysis results are highly consistent with the finite element analysis (FEA) and the thrust density can reach over 10 MN/m^3. Subsequently, Pakdelian et al. [13] summarized the general design method of MLS, which can adjust the transmission ratio of the MLS by changing the number of poles of the spiral PMs and the lead of

Manuscript received 15 March 2024; revised 5 June 2024; accepted 4 July 2024. Date of publication 11 July 2024; date of current version 4 September 2024. This work was supported in part by the National Natural Science Foundation of China under Grant 41576096 and Grant 41876096, in part by the Youth Fund of Jiangsu Natural Science Foundation under Grant BK20201034, in part by the Natural Science Research Project of Jiangsu Higher Education Institutions under Grant 20KJB470028, and in part by the Scientific Research Fund of Nanjing Institute of Technology under Grant YKJ2019115. Recommended for publication by Associate Editor M. Vitelli. *(Corresponding author: Tao Xia.)*

Tao Xia, Zihao Li, Haitao Liu, and Yangfei Zhang are with the School of Electric Power Engineering, Smart Grid Research Institute, Nanjing Institute of Technology, Nanjing 210000, China (e-mail: shertown@163.com; 18862655737@163.com; htt1989411@163.com; yfzhang_njit@163.com).

Haitao Yu is with the Engineering Research Center for Motion Control of MOE, Southeast University, Nanjing 210000, China (e-mail: htyu@seu.edu.cn).

Color versions of one or more figures in this article are available at https://doi.org/10.1109/TPEL.2024.3424535.

Digital Object Identifier 10.1109/TPEL.2024.3424535

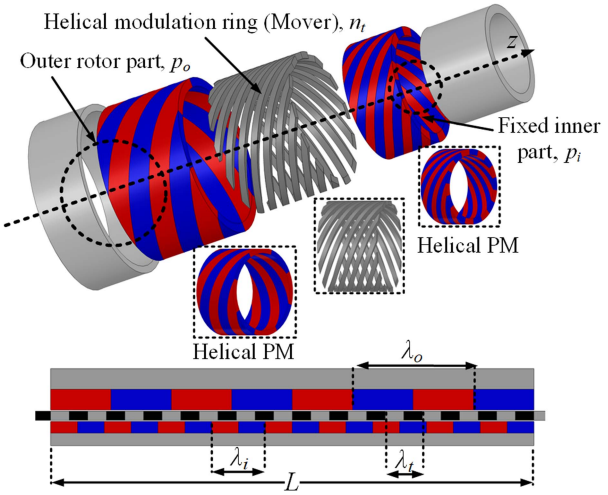

Fig. 1. MFMS with $p_i = 9$ pole–pairs, $p_o = 4$ pole pairs, and $n_t = 13$ pole pairs.

the MLS. Holm et al. [14] used MLS for wave energy conversion and designed a model with a thrust force of up to 17 kN, which was experimentally verified.

A magnetic field modulated screw (MFMS) was proposed in [15] and its structure is shown in Fig. 1. The device consists of an inner rotor, an outer cylinder (fixed), and an intermediate-layer spiral ferromagnetic ring, which saves the PM of the moving parts. MFMS is very suitable for long-distance applications. However, the design of the structure requires that both the inner and outer PMs are helical, which increases the difficulty and cost of manufacturing these PMs [16]. In addition, both the inner and outer PMs are surface mounted, increasing the complexity and size of the device. MLS needs to be combined with motors when applied in the energy conversion field [17], [18]. Ordinary surface-mounted MLS combined with motors will make the overall structure more complex and increase the size of the system. In addition, decoupling technology for the magnetic circuit inside and outside the rotor needs to be considered [19], [20], [21].

To solve the problems of existing MLS, this article proposes a segmented modulated MLS with a Halbach arrangement of inner stator magnets (Halbach-SMMLS). Due to the use of a ferromagnetic modulating ring as an actuator, the cost of PM material and spiral magnet processing will be saved in long-distance applications. In addition, by increasing the ratio of the ferromagnetic modulating ring to the number of poles of the outer rotor, a higher ratio of linear speed to rotational speed transmission can be realized. The circular PMs of the inner stator and the segmented helical magnets of the outer rotor greatly reduce the difficulty of machining the equipment and save machining costs. Due to the composite design of the magnetic spiral rotor and the motor rotor, the system structure is simplified and the overall volume of the device is reduced. The embedded structure protects the PM material from the impact of seawater and improves the service life of the device. Finally, the superiority of the proposed Halbach-SMMLS is verified by FEA and experiments. Table I lists a comparison of the characteristics of different magnetic actuators.

TABLE I
CHARACTERISTICS OF DIFFERENT MAGNETIC ACTUATORS

Magnetic actuators	RMG	LMG	MLS	MFMS	Halbach-SMMLS
Motion freedom	1	1	2	2	2
mover material	/	PM	PM	ferromagnet	ferromagnet
Rotor material	PM	/	PM	PM	PM
Inner PM	circular arc	cuboid	helical	helical	circular
Outer PM	circular arc	cuboid	helical	helical	Segmented helical
Layers (Mechanical to electrical)	3	2	3	3	1

II. Structural Design and Modulation Principles

A. Structural Design of Halbach-SMMLS

The Halbach-SMMLS consists of three coaxial tubular components: an inner stator, an intermediate modulation ring, and an outer rotor. Fig. 2(a) shows the overall structure of a surface-mounted modulated magnetic guide screw (SM-MMLS). Its inner stator is composed of a nontilted PM ring with a polar number of p_i. Magnet width is w_i. Lead λ_i is defined as twice the width of the magnet. The modulation ring in the middle layer is a ferromagnetic spiral structure with n_t pole pairs. The width of the ferromagnetic pole plate is w_t. Lead λ_t is defined as twice the width of the ferromagnetic pole plate, and the modulation loop is the translator of SM-MMLS. Fig. 2(b) shows the improvement process of SM-MMLS, which upgrades the PMs on the inner stator of SM-MMLS to a Halbach structure. Its outer rotor PMs are cut into helical PMs and, then, embed them into a nonmagnetic framework. The number of poles of the outer rotor is p_o. Magnet width is w_o. Lead λ_o is defined as twice the width of the magnet. The final structure of Halbach-SMMLS is shown in Fig. 2(c). Since the outer rotor PMs are helical, when they rotate, they generate a dynamic helical magnetic field that moves along the z-axis direction. The dynamic spiral magnetic field will be modulated by the middle layer ferromagnetic spiral ring, thus generating additional spatial harmonics, which will interact with the magnetic field generated by the inner stator magnet to generate axial thrust.

The Halbach-SMMLS converts the low-speed, high-thrust translational motion of a translator into a high-speed, low-torque rotational motion of a rotor. An important feature of this construction is the use of a ferromagnetic modulating ring in the actuator, which saves PM material in long-distance applications and improves the ratio of n_t to p_o, resulting in a higher transmission ratio. The nontilted PM ring structure of the inner stator and the segmented helical magnet structure of the outer rotor reduce the difficulty of machining PM material and save machining costs. Due to the composite design of the magnetic spiral rotor and the motor rotor, the system structure is simplified and the overall size of the equipment is reduced. The embedded

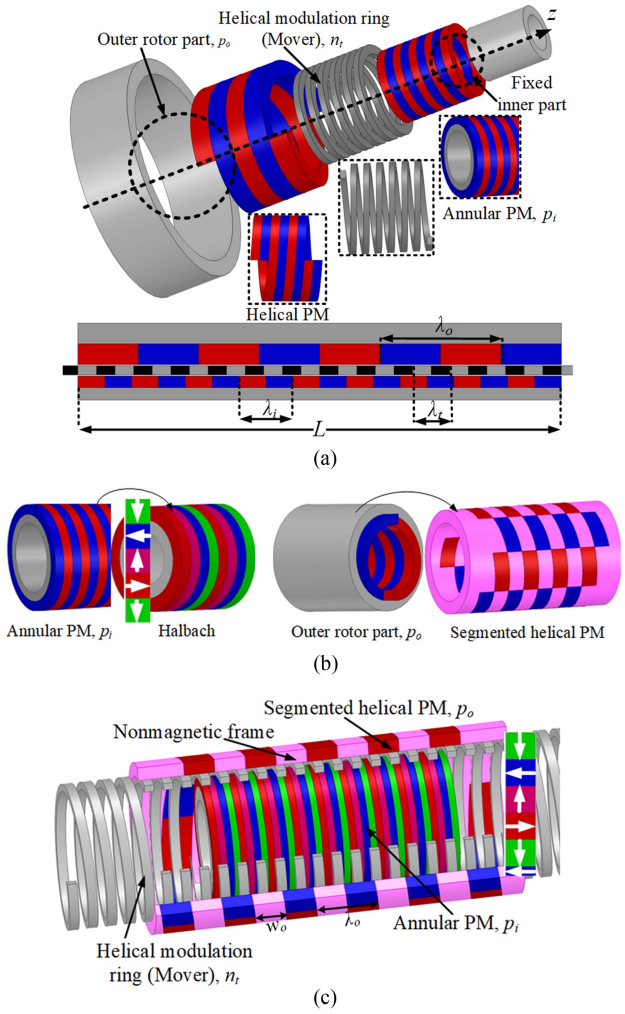

Fig. 2. Topologies. (a) Surface-mounted modulated MLS (SM-MMLS). (b) Improvement process of SM-MMLS. (c) Segmented modulated MLS with Halbach structure (Halbach-SMMLS).

structure protects the PM material from the impact of seawater and improves the service life of the equipment.

B. Modulation Principle of Halbach-SMMLS

To achieve matching of thrust and torque, an ordinary MLS requires the same number of magnetic poles for both the nut and the screw. However, the proposed Halbach-SMMLS can increase the transmission ratio by changing the number of magnetic poles of different components. According to the magnetic field modulation theory, the relationship between the magnetic pole pairs of the inner stator, the intermediate modulating ring and the outer rotor in the Halbach-SMMLS can be derived as follows:

$$n_t = p_i + p_o. \tag{1}$$

In the axial analysis, the relationship between the lead and pole pairs of each part is

$$p_i = \frac{L}{\lambda_i}, p_o = \frac{L}{\lambda_0}, n_t = \frac{L}{\lambda_t} \tag{2}$$

where L is the effective axial length, λ_i is the lead of the inner stator PMs, λ_o is the lead of the outer rotor PMs, and λ_t is the lead of the rotor spiral modulation ring. Due to the equal axial effective lengths of the three parts, the correlation expression for the product of the lead and polar logarithm of each part can be obtained as

$$\lambda_i p_i = \lambda_o p_o = \lambda_t n_t. \tag{3}$$

In circumferential analysis, the relationship between the leads and polar logarithms of the three parts must be suitable for a radian of one cycle. The circumferential relationship between the Halbach-SMMLS lead and the number of poles is obtained using the definition of the transmission ratio of a common MLS. For an ordinary MLS, when the magnetic nut is rotated one pole distance, the magnetic actuator is moved one pole distance accordingly. Because the pole distances of magnetic nuts and MLS are expressed in different units, the linear speed to rotational speed transmission ratio is generated during the calculation process. The transmission ratio is defined as the ratio of the rotor angular velocity ω (rad/s) to the translational linear velocity V (m/s) given by

$$G = \frac{\omega}{V} = \frac{2\pi}{\lambda}. \tag{4}$$

In the ordinary MLS, the various parts of λ are equal; however, in Halbach-SMMLS, due to the different polar pairs of each part, the lead of each part is not equal. The transmission ratio needs to be derived using wavenumbers, and the wavenumbers of each part must meet the circumferential relationship between lead and polar logarithms. The definition of wavenumbers is as follows:

$$k_i = \frac{2\pi}{\lambda_i}, k_o = \frac{2\pi}{\lambda_o}, k_t = \frac{2\pi}{\lambda_t}. \tag{5}$$

The rotating part of Halbach-SMMLS is the outer rotor, and (5) is taken into (4) to obtain

$$\omega_o = \frac{2\pi}{\lambda_o} V_o = k_o V_o. \tag{6}$$

Bring (2) into (5) to obtain

$$k_i = \frac{2\pi p_i}{L}, k_o = \frac{2\pi p_o}{L}, k_t = \frac{2\pi n_t}{L}. \tag{7}$$

Due to p_i and p_o, n_t satisfies (1), thus obtaining

$$k_t = k_i = k_o. \tag{8}$$

When the outer rotor rotates, it generates a dynamic helical magnetic field that moves along the z-axis direction. The dynamic spiral magnetic field will be modulated by the middle layer ferromagnetic spiral ring. If (1) is satisfied, the modulated helical magnetic field will interact with the internal stator PMs to generate axial thrust, thereby driving the linear motion of the modulated ring. The study of the linear speed to rotational speed transmission ratio requires the use of a speed formula for magnetic field modulated linear gears, which is given in [16] and is defined as follows:

$$p_o V_o = n_t V_t - p_i V. \tag{9}$$

Substituting (3) and (6) into (9) yields

$$\omega_o = \frac{k_o\lambda_o}{\lambda_t}V_t - \frac{k_o\lambda_o}{\lambda_i}V_i. \tag{10}$$

It can be noted that

$$k_0\lambda_0 = 2\pi. \tag{11}$$

Using (5), (10) can be simplified as

$$\omega_o = k_tV_t - k_iV_i. \tag{12}$$

In Halbach-SMMLS, the inner cylinder remains fixed and $V_i = 0$, then

$$\omega_o = k_tV_t = \frac{2\pi}{\lambda_o}\frac{n_t}{p_o}V_t. \tag{13}$$

This reflects that Halbach-SMMLS can convert the linear speed of the spiral ferromagnetic ring into the rotational speed of the outer rotor.

Under static conditions, the axial thrust on the three components of Halbach-SMMLS needs to meet the following conditions:

$$F_i + F_t + F_o = 0 \tag{14}$$

where F_i is the stator thrust, F_t is the helical magnetic ring thrust, and F_o is the rotor thrust. At the same time, due to the helical structure of the magnetic regulating ring and the outer PMs of the rotor, torque is generated on these two components, which is related by the following equation:

$$T_o + T_t = 0 \tag{15}$$

where T_o is the external rotor torque, and T_t is the torque of the spiral magnetic ring. Due to the circular structure of the inner stator, it does not tilt, so it will not be subjected to any torque.

Based on the law of conservation of energy transfer, In Halbach-SMMLS, the power associated with the translator motion, P_t equals the power associated with the rotor rotation P_o. From this, the relationship between the translator thrust and rotor torque can be obtained

$$P_t = P_o \Rightarrow F_tV_t = T_o\omega_o \Rightarrow \frac{F_t}{T_o} = \frac{\omega_o}{V_t} = \frac{2\pi}{\lambda_o}\frac{n_t}{p_o}. \tag{16}$$

It can be seen that the linear velocity of the helical ferromagnetic ring can be converted into the rotational speed of the outer rotor, whereas the thrust of the translator can be converted into the torque of the rotor. The transmission ratio of the Halbach-SMMLS depends on the pole–pair ratio of the outer rotor and the helical magnetic ring. The speed increase effect is achieved by changing the pole–pair ratio. Since the helical magnetic ring is made entirely of low-cost ferromagnetic material, the linear stroke of the actuator is increased without the need for more PM material, thus saving on the material costs of the device.

III. Design Optimization and Performance Analysis

A. Design Optimization

To evaluate the performance of Halbach-SMMLS compared to the previously studied MFMS and MLS, the surface-mounted modulated magnetically guided screw (SM-MMLS) was first optimally designed as shown in Fig. 3, with the outer radius $r_o = 37$ mm and axial length selected as $L = 100$ mm. The pole combination selected for the SM-MMLS is $(p_i, p_o, n_t) = (9, 4, 13)$. This yields a gear ratio $G = 817$ m^{-1} ($2\pi\times13/0.1$ m), so the translator thrust is amplified 817 times relative to the torque applied to the rotor.

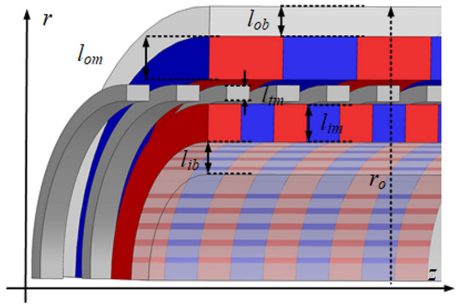

Fig. 3. Cross-sectional dimensional parameters of SM-MMLS.

TABLE II
Initial Dimensions and Design Variables of SM-MMLS

Parameter	Definition	Setpoint	Scope
l_{ib}(mm)	Inner iron height	5.0	3.0–7.5
l_{im}(mm)	Inner PM height	5.5	3.0–7.5
l_{ob}(mm)	Outer iron height	5.5	/
l_{om}(mm)	Outer PM height	5.5	3.0–7.5
l_{tm} (mm)	Modulation ring height	3.0	2.6–6.2

Use 3-D FEA iterative parameter scanning analysis to determine the optimal structure of SM-MMLS. The goal is to determine the maximum values of peak thrust and peak torque at a fixed outer radius. Some of the parameters of the SM-MMLS have already been determined. Now only the remaining radial parameters need to be optimized, i.e., inner stator back-iron thickness l_{ib}, inner stator magnet thickness l_{im}, outer rotor back-iron thickness l_{ob}, outer rotor magnet thickness l_{om}, and ferromagnet modulating ring thickness l_{tm}. Fig. 3 shows the local parameter model of the SM-MMLS. Table II lists the optimization variables, initial values, and optimization ranges. The initial values are determined by the fixed outer radius of the SM- MMLS and the number of pole pairs for a fixed shaft length L.

Fig. 4 shows the corresponding relationship between the peak thrust and the design variables (internal magnet thickness l_{im} and external magnet thickness l_{om}). In this iteration, l_{im} and l_{om} perform parameter scanning and the remaining parameters of SM-MMLS are fixed. Determine that the peak force occurs at $(l_{im}, l_{om}) = (3.5, 4.5)$ mm.

The optimal solution for the thickness of the inner and outer magnets is obtained through Fig. 4, which is fixed, and then the thickness l_{tm} of the ferromagnetic modulating ring is adjusted for parameter scanning, and the scanning results are shown in Fig. 5. It can be seen that the peak thrust decreases with the increase of the thickness l_{tm} of the ferromagnetic modulating ring. In addition, when l_{tm} is larger than 3 mm and continues to increase, the peak thrust decreases faster. Considering that the ferromagnetic modulating ring plays the role of a translator in

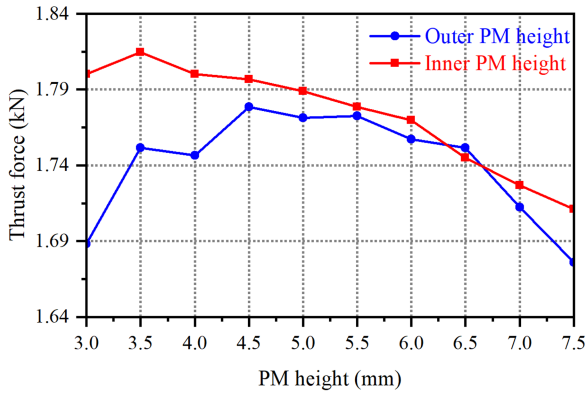

Fig. 4. Peak thrust change due to changes in the thickness of internal and external magnets.

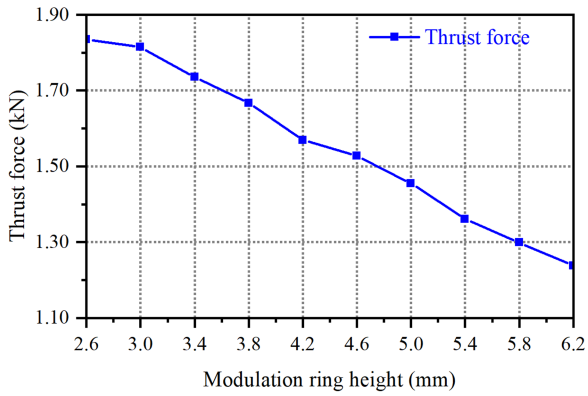

Fig. 5. Peak thrust change caused by changes in the thickness of the intermediate layer modulation ring.

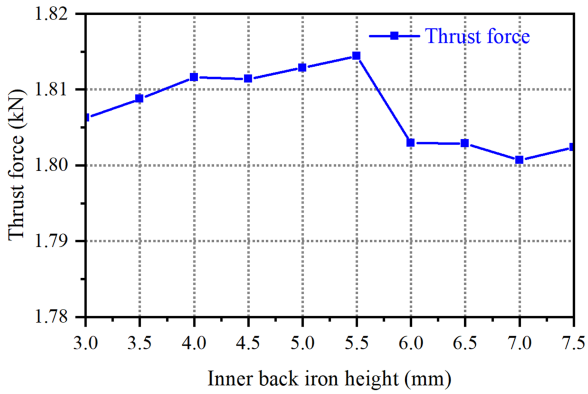

Fig. 6. Peak thrust change caused by changes in the thickness of the inner stator back iron.

TABLE III
INITIAL DIMENSIONS AND DESIGN VARIABLES OF SM-MMLS

Parameter	Value
Outer radius, r_o(mm)	37
Active length, L (mm)	100
Pole–pairs of inner part, p_i	9
Pole–pairs of modulator, n_t	13
Pole–pairs of outer part, p_o	4
Air-gap length, g (mm)	1
Inner PM height, l_{im} (mm)	3.5
Teeth height, l_{tm} (mm)	3.0
Outer PM height, l_{om}(mm)	4.5
Inner back iron height l_{ib} (mm)	5.5
PM material	Nd-Fe-B
PM remanent (T)	1.23

SM-MMLS and has to withstand a large impact force in application scenarios such as wave power generation, the thickness of the ferromagnetic modulating ring l_{tm} is selected as 3 mm based on the considerations of the peak thrust and impact resistance of the ferromagnetic modulating ring.

In the final structure of Halbach-SMMLS proposed in this article, the outer rotor magnets are embedded in segments. Therefore, the outer rotor backing iron thickness l_{ob} will no longer be optimized, and only the inner stator backing iron thickness l_{ib} will be optimized. The calculation results of l_{ib} are shown in Fig. 6. It can be seen that the influence of the inner stator backing iron thickness l_{ib} on the peak thrust is very small, and the maximum value of the thrust is obtained at $l_{ib} = 5.5$ mm. Parameters of the optimized SM-MMLS are listed in Table III.

B. Harmonic Analysis

According to the magnetic field modulation theory, harmonic shifts can be realized in the axial direction when the pole pairs of the inner stator, the intermediate modulating ring, and the outer rotor satisfy (1). 3-D finite element simulations are performed to calculate the axial harmonic content in the inner and outer air gaps and to verify the harmonic shifts. The axial flux density induced by the helical PM in the vicinity of the outer rotor is first evaluated using the final values given in Table III. The structure without a modulating ring is shown in Fig. 7(a), the axial flux density waveform is shown in Fig. 7(b), and the corresponding space harmonics are shown in Fig. 7(c). It shows that the 4th harmonic mainly exists in the external air gap.

When the circular PM on the internal stator acts alone, the same type of diagram in the internal air gap is shown in Fig. 8. As can be seen from Fig. 8(c), it is mainly the 9th harmonic wave in the internal air gap.

When the spiral PM of the outer rotor coexists with the modulating ring, the structure in Fig. 9(a)–(c) shows the magnetizing effect of the modulating ring, indicating that the helical PM of the outer rotor is modulated to generate the necessary 9th harmonic in the internal air gap. This 9th harmonic interacts with the 9th harmonic originally present in the internal air gap to achieve thrust transfer. The corresponding inner ring PM is modulated to generate a new 4th harmonic in the external air gap. The new 4th harmonic interacts with the existing 4th harmonic in the external air gap to achieve thrust transfer.

Therefore, if magnetic field coupling is to be established inside the MLS, the pole pairs of the inner stator, intermediate modulation ring, and outer rotor must satisfy (1), which is consistent with the theoretical analysis results.

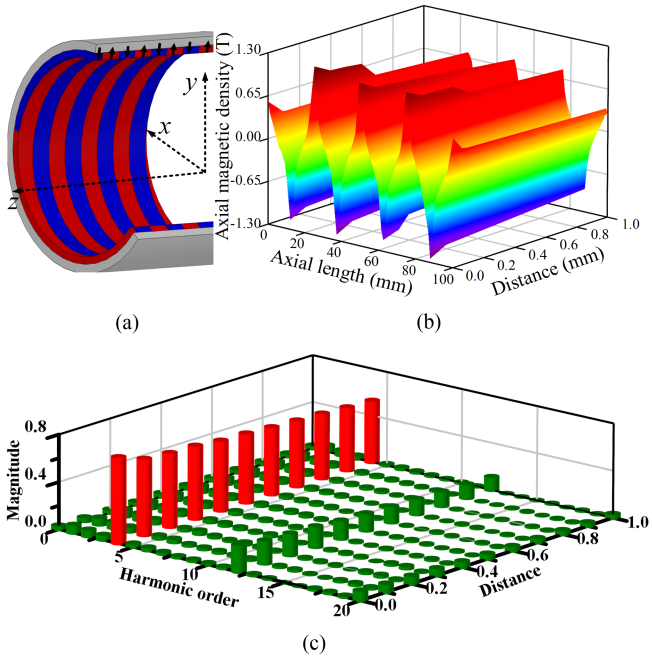

Fig. 7. External magnet acting alone. (a) Structure. (b) Axial magnetic density. (c) Harmonic order.

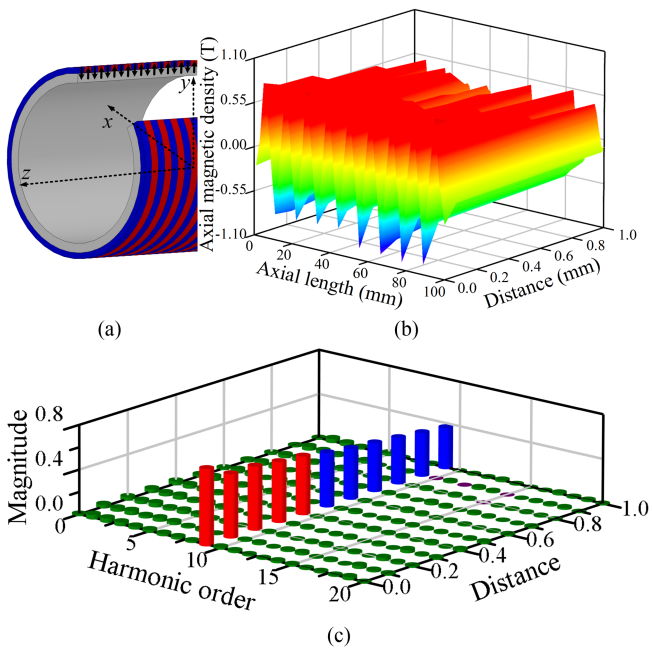

Fig. 8. Internal magnet acting alone. (a) Structure. (b) Axial magnetic density. (c) Harmonic order.

C. Performance Analysis

The internal stator of the SM-MMLS is a nontilted PMs circular structure, which reduces the processing difficulty of PM materials and saves processing costs. However, the thrust performance of the circular magnets compared to the screw magnets needs to be further investigated. The MFMS is shown in Fig. 10. The internal stator of this structure consists of helical

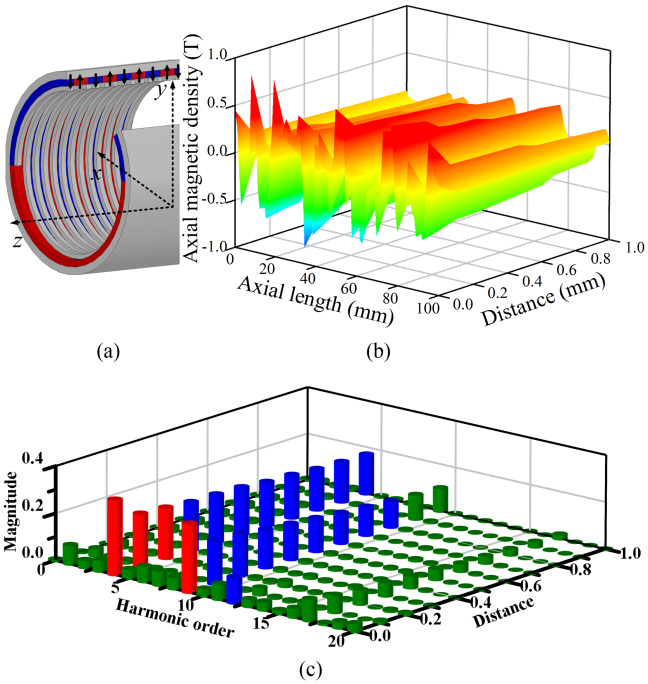

Fig. 9. External magnet and modulation ring work together. (a) Structure. (b) Axial magnetic density. (c) Harmonic order.

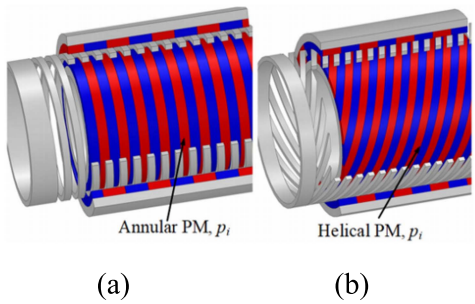

Fig. 10. Different structures (a) SM-MMLS. (b) MFMS.

PMs. 3-D FEA was used to compare the thrust performance of SM-MMLS and MFMS. From Fig. 11, it can be seen that the peak thrust of SM-MMLS is 1.83 kN, whereas the peak thrust of MFMS is 1.60 kN. In addition, the ratio of this MFMS is only 205 m^{-1}, whereas that of the SM-MMLS proposed in this article is 817 m^{-1}.

As the outer rotor of the SM-MMLS rotates and the other components remain stationary, torque and axial force along the Z-axis are generated. The axial thrust obtained by each component is related to the number of poles. Since the stator is not tilted, it is not subjected to any torque. Figs. 12 and 13 show the calculated axial thrust and torque, respectively. Fig. 14 shows the axial thrust acting on the translator and the torque acting on the outer rotor when the outer rotor is rotating alone. It can be seen that the ratio of thrust on the translator to torque on the outer rotor is 817 m^{-1}, which agrees with the derivation of the transmission ratio in (16).

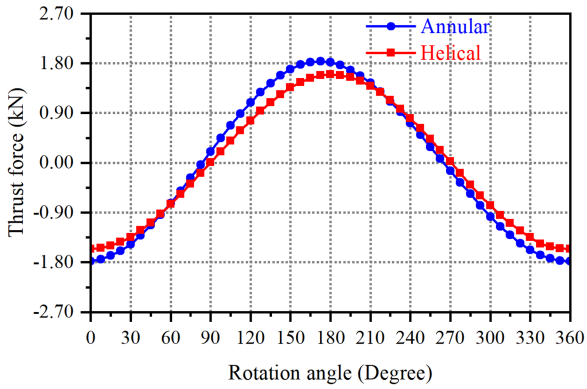

Fig. 11. Thrust force on the modulation ring.

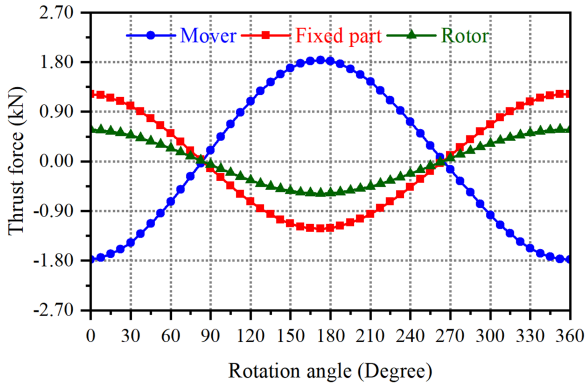

Fig. 12. Thrust on each part due to the rotation of the outer rotor.

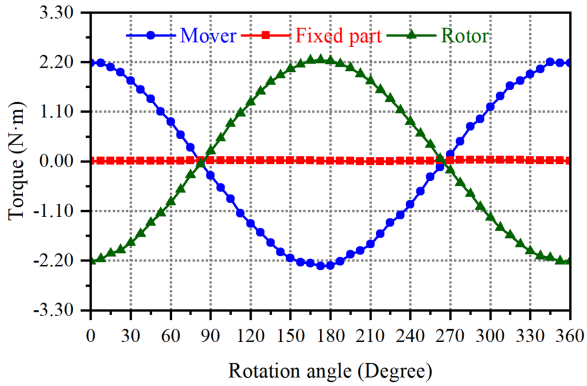

Fig. 13. Torque applied to each part due to the rotation of the outer rotor.

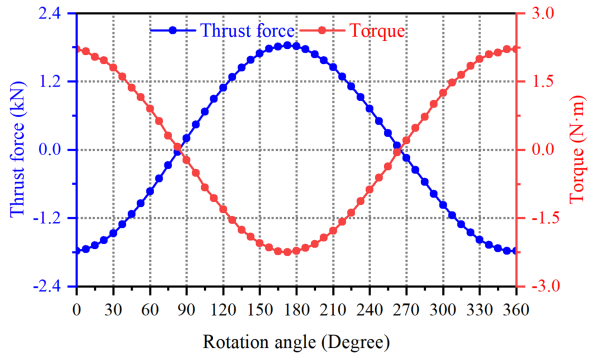

Fig. 14. Torque on the outer rotor and the thrust on the modulation ring due to the rotation of the outer rotor.

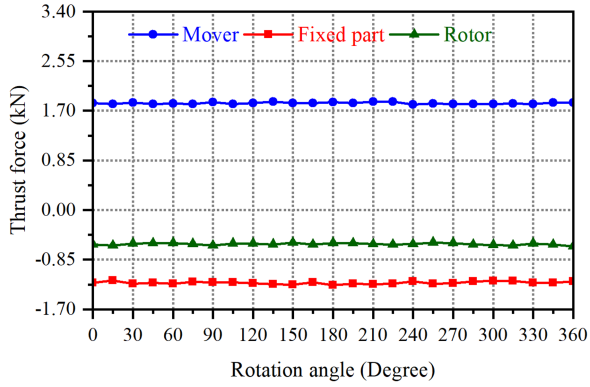

Fig. 15. Thrust on each part when the outer rotor is rotating at $\omega_o = 390$ r/min and the translator moves at $v_t = 0.05$ m/s.

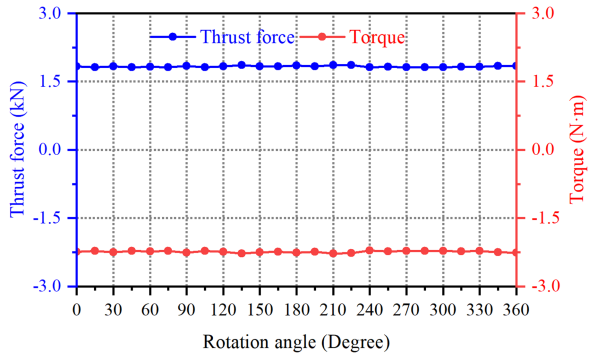

Fig. 16. Thrust on the translator and torque on the outer rotor when the outer rotor is rotating at $\omega = 390$ r/ min and the translator moves at $v_t = 0.05$ m/s.

When the outer rotor is rotating at $\omega_o = 390$ r/min and the translator is moving at $v_t = 0.05$ m/s, the torque and force calculated for the SM-MMLS are shown in Fig. 15, where it can be seen that the value of the thrust force acting on each component remains more or less the same due to the matching of the outer rotor speed with the translator linear velocity. Fig. 16 shows the axial thrust force acting on the translator and the torque of the outer rotor as the outer rotor rotates and the translator moves. It can be seen that the thrust and torque remain essentially constant near their peak values. To generate a force of 1.83 kN on the translator, only 2.24 N·m of torque is required. The ratio of thrust on the translator to torque on the outer rotor is 817 m^{-1}. The proposed design also exhibits very low torque fluctuations.

D. Quantitative Comparison

Due to the complexity of the structure of the SM-MMLS when combined with the motor, the helical PMs of the outer rotor of the SM-MMLS are changed to a segmented embedded type, which would weaken the thrust performance of the device. To compensate for the thrust, the internal stator PMs of the device

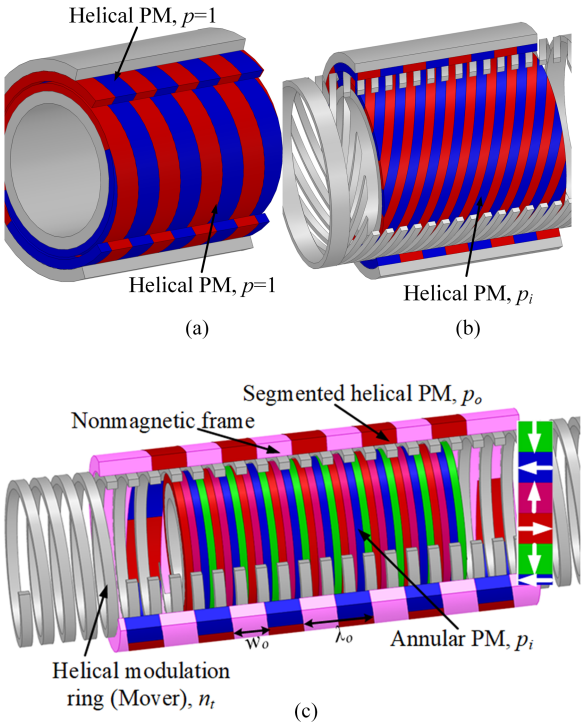

Fig. 17. Different magnetic screw topologies. (a) MLS. (b) MFMS. (c) Halbach-SMMLS.

TABLE IV
VARIOUS VALUES OF THREE STRUCTURES

	MLS	MFMS	H-SMMLS
Outer radius, r_o (mm)		37	
Active length, L (mm)		100	
Pole–pairs of inner part, p_i	4	9	9
Pole–pairs of outer part, p_o	4	4	4
Inner PM height, l_{im} (mm)		3.5	
Outer PM height, l_{om} (mm)		4.5	
Thrust force (kN)	3.01	1.60	1.44
Inner part torque (N·m)	14.30	7.80	1.76
Gear ratio (m^{-1})	210	205	817

are designed as a Halbach flux-gathering structure, as shown in Fig. 17(c).

The thrust values of MLS, MFMS, and Halbach-SMMLS were compared through 3-D FEA. The thrust calculation results are shown in Table IV.

It can be seen that the MLS has the highest peak thrust for the same design parameters because the MLS has only one layer of air gap. However, the input torque of the MLS is 14.3 N·m, which is much larger than that of the MFMS and Halbach-SMMLS. In addition, the cost of the MLS actuator PM material increases in long-range applications. The Halbach-SMMLS has the highest gear ratio of the three configurations at 817 m^{-1}. The thrust of the Halbach-SMMLS is reduced by about 10% compared to the MFMS. However, the segmented embedded structure of the Halbach-SMMLS outer rotor PMs allows it to be directly nested with the motor to form a composite rotor, reducing the size and manufacturing cost of the composite motor back unit. In addition, the embedded PMs are protected from seawater impact and erosion, thereby increasing the service life of the device.

TABLE V
MATERIAL PRICES AND CONSUMPTION

	MLS	MFMS	H-SMMLS
Mover material (USD/kg)	NdFeB: 85	B20AT: 1.32	DW540: 0.76
B20AT consumption (kg)	/	0.177	/
DW540 consumption (kg)	1.446	1.339	1.169
NdFeB consumption (kg)	1.020	0.971	0.793
Cost of materials (USD)	87.799	83.786	68.293

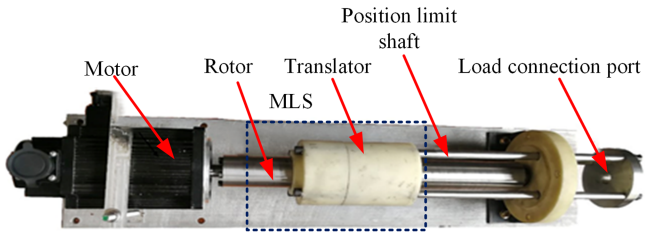

Fig. 18. Top view of the manufactured MLS.

To further evaluate the performance of magnetic actuators, it is necessary to consider the linear motion distance, material consumption, manufacturing difficulty, and transmission performance in real-world applications. The material prices, material consumption, and total material costs for each component of the three devices are listed in Table V. The MLS is very expensive to manufacture because the PM of its actuator increases exponentially with the distance traveled. Compared to the MLS and MFMS, the Halbach-SMMLS consumes 22.3% and 18.3% less PM, respectively. The segmented embedded structure of the Halbach-SMMLS outer rotor PM allows it to be nested in the motor to form a composite rotor. PM consumption is reduced by 33.9% and 32.0%, respectively, when the outer rotor PM thickness is 4 mm. PM for MLS and MFMS is typically cut at an angle and then spliced to approximate a helix, increasing manufacturing costs and installation difficulties [21]. The internal ring magnets and external embedded segmented magnets of the Halbach-SMMLS are much less difficult to manufacture and install. The embedded PM material also protects against seawater impact and erosion, thus extending the service life of the equipment. Therefore, considering the transmission performance, size, and manufacturing cost, the Halbach-SMMLS structure proposed in this article has significant advantages.

IV. EXPERIMENT VERIFICATION

Based on the above analysis, it can be found that the magnetic drive can realize noncontact high-efficient conversion. To verify the theoretical analysis of the magnetic drive technology, a prototype of the MLS was made and tested, as shown in Fig. 18. In this MLS, the PMs are made of rare-earth material N38 NdFeB, and the core material DW470-50 is used for the rotor back-iron and rotor back-iron. To measure the thrust characteristics of the MLS, a rotating crankshaft platform was fabricated for the thrust test. In this device, one end of the crankshaft linkage is connected

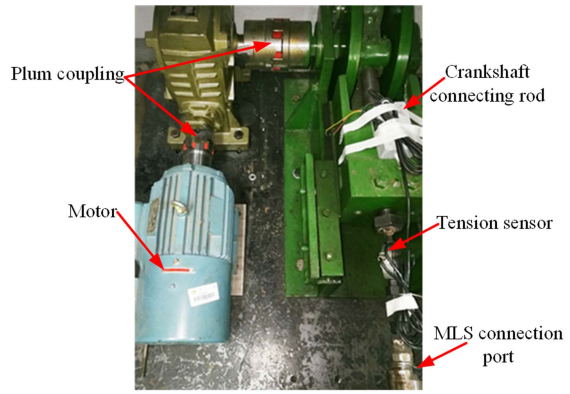

Fig. 19. Experimental platform.

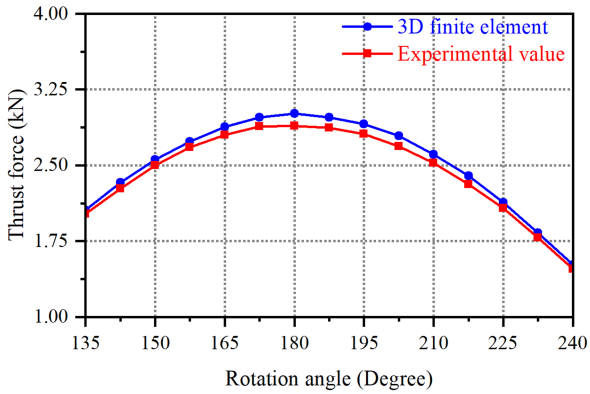

Fig. 20. Thrust changes between the theoretical and measured values.

to the drive motor through two plum couplings, and the other end is connected to the moving element of the MLS through a tension sensor. At this point, the experimental test platform was constructed as shown in Fig. 19.

The rotor is first fixed, and the drive motor is started to drive the crankshaft linkage, which drives the mover of the MLS to move. The relative positions of the PMs on the rotor and the mover change, resulting in thrust and torque. The tension sensor senses the change in force and converts it into an electrical signal output.

Fig. 20 compares the thrust changes between the theoretical and measured values. It can be seen that there is good consistency between the predicted and measured results. The peak thrust obtained from 3-D FEA is 3.01kN, while the measured peak thrust is 2.89kN. The measured value decreased by 3.7% compared to the 3-D FEA results, which is caused by the uneven fitting of the spiral magnet.

V. Conclusion

This article describes the structure and operational characteristics of the Halbach-SMMLS. The effect of the magnetic field modulation technique on torque and thrust is investigated. The performance of the Halbach-SMMLS is demonstrated to be superior to that of the previously proposed MFMS and MLS through 3-D FEA. The advantages of the Halbach-SMMLS are shown to be lower PMs machining difficulty and cost, better suited for low-speed, high thrust, long-distance applications such as wave energy conversion, and smaller size when nested in a motor. Finally, an MLS prototype was constructed to verify the 3-D magnetic field transfer mechanism.

References

[1] M. C. Gardner, B. Praslicka, M. Johnson, and H. A. Toliyat, "Optimization of coaxial magnetic gear design and magnet material grade at different temperatures and gear ratios," *IEEE Trans. Energy Convers.*, vol. 36, no. 3, pp. 2493–2501, Sep. 2021.

[2] L. Jing, Z. Huang, J. Chen, and R. Qu, "Design, analysis, and realization of a hybrid-excited magnetic gear during overload," *IEEE Trans. Ind. Appl.*, vol. 56, no. 5, pp. 4812–4819, Sep./Oct. 2020.

[3] S. Mirnikjoo, F. Asadi, K. Abbaszadeh, and S. E. Abdollahi, "Effect of rotor topology on the performance of counter-rotating double-sided flux switching PMs generator," *IEEE Trans. Energy Convers.*, vol. 37, no. 1, pp. 65–74, Mar. 2022.

[4] H. T. Faus, "Magnet gearing," U.S. Patent 2243555, May 27, 1941.

[5] J. Zhou, M. Cheng, H. Wen, X. Yan, M. Tong, and W. Wang, "Modeling and suppression of torque ripple in PMSM based on the general airgap field modulation theory," *IEEE Trans. Power Electron.*, vol. 37, no. 10, pp. 12502–12512, Oct. 2022.

[6] J. Bai, J. Liu, G. Liu, Y. Liu, and P. Zheng, "Investigation of the power factor of magnetic-field modulated brushless double-rotor machine," *IEEE Trans. Power Electron.*, vol. 36, no. 1, pp. 423–432, Jan. 2021.

[7] Z. Yu, C. Gan, Y. Chen, and R. Qu, "DC-biased sinusoidal current excited switched reluctance motor drives based on flux modulation principle," *IEEE Trans. Power Electron.*, vol. 35, no. 10, pp. 10614–10628, Oct. 2020.

[8] K. Atallah, S. D. Calverley, and D. Howe, "Design, analysis and realisation of a high-performance magnetic gear," *IEE Proc., Electr. Power Appl.*, vol. 151, no. 2, pp. 135–143, 2004.

[9] W. Li, K. T. Chau, and J. Z. Jiang, "Application of linear magnetic gears for pseudo-direct-drive oceanic wave energy harvesting," *IEEE Trans. Magn.*, vol. 47, no. 10, pp. 2624–2627, Oct. 2011.

[10] K. Atallah, J. Wang, and D. Howe, "A high-performance linear magnetic gear," *J. Appl. Phys.*, vol. 97, no. 10, May 2005, Art. no. 10N516.

[11] N. G. Vitale, G. B. Hirschman, and W. A. Smith, "Optimization of drive screw pitch in a pulsatile ventricle assist device," in *Proc. IEEE 27th Annu. Northeast Bioeng. Conf.*, 2001, pp. 37–38.

[12] J. Wang, K. Atallah, and W. Wang, "Analysis of a MLS for high force density linear electromagnetic actuators," *IEEE Trans. Magn.*, vol. 47, no. 10, pp. 4477–4480, Oct. 2011.

[13] S. Pakdelian, N. W. Frank, and H. A. Toliyat, "Principles of the trans-rotary magnetic gear," *IEEE Trans. Magn.*, vol. 49, no. 2, pp. 883–889, Feb. 2013.

[14] R. K. Holm, N. I. Berg, M. Walkusch, P. O. Rasmussen, and R. H. Hansen, "Design of a MLS for wave energy conversion," *IEEE Trans. Ind. Appl.*, vol. 49, no. 6, pp. 2699–2708, Nov./Dec. 2013.

[15] Z. Ling, W. Zhao, J. Ji, and M. Xu, "Design and analysis of a magnetic field screw based on 3-D magnetic field modulation theory," *IEEE Trans. Energy Convers.*, vol. 37, no. 4, pp. 2620–2628, Dec. 2022.

[16] M. Bahrami Kouhshahi, J. Z. Bird, J. D. Kadel, and W. B. Williams, "Designing and experimentally testing a magnetically geared lead screw," *IEEE Trans. Ind. Appl.*, vol. 54, no. 6, pp. 5736–5747, Nov./Dec. 2018.

[17] G. Liu, L. Fang, Z. Liu, Q. Chen, and J. Zhang, "Active disturbance rejection control of a magnetic screw motor for high tracking performance," *IEEE Trans. Power Electron.*, vol. 37, no. 8, pp. 9641–9651, Aug. 2022.

[18] Z. Ling, J. Ji, F. Wang, and F. Bian, "Design and analysis of a field modulated MLS for artificial heart," *AIP Adv.*, vol. 7, no. 5, May 2017, Art. no. 056717.

[19] C. S. Cyusa and Y. Fujimoto, "Enactment-based direct-drive test of a novel radial-gap helical RotLin machine," *IEEE Trans. Ind. Appl.*, vol. 54, no. 2, pp. 1273–1282, Mar./Apr. 2018.

[20] Z. Ling, W. Zhao, P. O. Rasmussen, J. Ji, Y. Jiang, and Z. Liu, "Design and manufacture of a linear actuator based on MLS transmission," *IEEE Trans. Ind. Electron.*, vol. 68, no. 2, pp. 1095–1107, Feb. 2021.

[21] Z. Ling, J. Ji, J. Wang, and W. Zhao, "Design optimization and test of a radially magnetized MLS with discretized PMs," *IEEE Trans. Ind. Electron.*, vol. 65, no. 9, pp. 7536–7547, Sep. 2018.

Tao Xia received the Ph.D. degree in electrical engineering from Southeast University, Nanjing, China, in 2019.

He was a joint Ph.D. student with Aalborg University. He is currently at Nanjing Institute of Technology, Nanjing, China. His research interests include ocean wave power generation, energy storage, and wind energy conversion.

Zihao Li was born in Huaian, China. He is currently working toward the M.S. degree in electrical engineering with the Nanjing Institute of Technology, Nanjing, China.

His current research focuses on wave power generation technology.

Haitao Liu received the Ph.D. degree in electrical engineering from Southeast University, Nanjing, China, in 2009.

She is currently a Professor with the Nanjing Institute of Technology, Nanjing, China. Her research interests include power system stability, energy storage, and power quality analysis.

Yangfei Zhang was born in Shenyang, China. He received the Ph.D. degree in electrical engineering from Hohai University, Nanjing, China, in 2009.

He is currently a Professor with the Nanjing Institute of Technology, Nanjing, China. His research interests include wind energy conversion, energy storage, and power system analysis.

Haitao Yu received the Ph.D. degree in electronics engineering from Huazhong University of Science and Technology, Wuhan, China, in 1995.

In 2003, he joined Southeast University as a Professor in the School of Electrical Engineering. His research interests include wave energy conversion and linear motor systems.